Journal of Environmental Management 404 (2026) 129576

Contents lists available at ScienceDirect

Journal of Environmental Management

journal homepage: www.elsevier.com/locate/jenvman

Research article

NH_3 slip identification and NH_3-Induced bias correction in remote NOx emissions monitoring of heavy-duty diesel vehicles

Chuntao Liu [a], Chenxi Wang [b,*], Zhiqiang Li [a], Yiqiang Pei [a,c], Chunling Wu [d], Fan Zhang [c], Jing Qin [c]

[a] School of Mechanical Engineering, Tianjin Renai College, Tianjin, 300392, China
[b] Institute for Transport Studies, University of Leeds, Leeds, LS2 9JT, UK
[c] State Key Laboratory of Engines, Tianjin University, Tianjin, 300072, China
[d] CATARC Automotive Test Center Company Limited, Tianjin, 300399, China

ARTICLE INFO

Keywords:
NH_3 slip detection
NOx sensor correction
Heavy-duty diesel vehicles
Telematics-integrated monitoring
Sliding-window algorithm

ABSTRACT

Remote in-use emissions monitoring of heavy-duty diesel vehicles (HDDVs) is increasingly adopted to strengthen air-quality governance and ensure real-world compliance with nitrogen oxides (NOx) limits. A persistent challenge is the severe cross-sensitivity of electrochemical NOx sensors to ammonia (NH_3) slip from aftertreatment systems. This interference inflates apparent NOx emissions, triggers false exceedances, and undermines the credibility of fleet-scale monitoring data. Here, a telematics-integrated dual-algorithm framework is proposed to detect NH_3 slip events and correct the NOx measurement bias resulting from NH_3-induced cross-sensitivity using only on-board signals, enabling scalable deployment without hardware modification. NH_3 slip is first identified using a moving-window NH_3 excess index (EI_{NH3}) combined with SCR efficiency thresholds to ensure robust event discrimination under transient driving. Cross-sensitivity artifacts are then corrected by constraining the effective selective catalytic reduction conversion to 99% during slip conditions and applying state compensation derived from Arrhenius-type NH_3 storage kinetics. The framework is validated on multiple HDDVs over real-driving emission (RDE) cycles using portable emissions measurement systems (PEMS) and a laser spectroscopic NH_3 analyzer as independent references. Results show that motorway high-speed operation exacerbates NH_3 slip under elevated space velocity and exhaust temperature. Across RDE tests, the identification module achieves 77-97% slip event recall and >93% classification accuracy, while the correction reduces the mean error of the 90th-percentile specific NOx emission (SE_{NOx}_P90) by 94% (0.50 to 0.03 g/kWh), effectively eliminating false exceedances attributable to NH_3 interference. In multi-vehicle compliance screening, several vehicles that would have been falsely flagged as non-compliant based on raw remote NOx data were reclassified as compliant after correction, with their estimated emissions falling below the 0.69 g/kWh regulatory limit, reducing false non-compliance determinations and improving the precision of high-emitter targeting. By enabling scalable and trustworthy NOx quantification, the proposed framework enhances the credibility and cost-effectiveness of telematics-based oversight. It supports cleaner freight operations through more reliable, data-driven emissions governance under real-world driving conditions.

1. Introduction

The global transportation sector faces intensifying pressure to advance emission-reduction technologies amid increasingly stringent worldwide regulations. Despite policy incentives promoting zero-emission alternatives, battery electric and hydrogen fuel cell vehicles still face substantial infrastructure and cost barriers (Komnos et al., 2025; Zhang et al., 2023), thereby sustaining the dominance of heavy-duty diesel vehicles (HDDVs) in freight transportation networks (Engelmann et al., 2021). The disproportionate contribution of HDDVs to nitrogen oxide (NOx) emissions necessitates urgent improvements in real-world emission-control compliance (Xu et al., 2023). Although the HDDVs equipped with selective catalytic reduction (SCR) systems can achieve >95% NOx conversion efficiency under standardized laboratory certification cycles, the real-world deNOx performance of the SCR system often degrades under real driving emission (RDE) conditions due to

* Corresponding author.
E-mail address: c.wang2@leeds.ac.uk (C. Wang).

https://doi.org/10.1016/j.jenvman.2026.129576
Received 15 January 2026; Received in revised form 2 March 2026; Accepted 2 April 2026
Available online 6 April 2026

transient engine loads and highly dynamic exhaust temperature and flow profiles (Liu et al., 2023; Jiang et al., 2022). Consequently, to ensure emissions compliance during actual operation, regulatory frameworks in China, the European Union, and the United States are advancing robust, scalable in-use NOx monitoring solutions to support more reliable compliance verification and data-driven air-quality management (Barbier et al., 2024; Yang et al., 2025; California Air Resources Board (CARB), 2021).

Current methodologies for monitoring NOx emissions from operational HDDVs face inherent limitations. Portable emission measurement systems (PEMS) provide reference-grade accuracy for RDE testing but remain impractical for large-scale fleet deployment due to their invasive installation requirements and prohibitive operational costs (Wang et al., 2020a). Alternative approaches, such as ambient air quality monitoring, on-road remote sensing, and tunnel studies, offer broader spatial coverage at reduced cost but are primarily directed toward aggregate regional air quality assessment rather than individual vehicle accountability (Helyar and Alnaggar, 2025; Smit et al., 2019; Huang et al., 2020). Additionally, these methods exhibit substantial weather-dependent variability that complicates data interpretation (Xia et al., 2022). Although plume-chasing techniques can target single-vehicle emissions, their reliability is fundamentally compromised by atmospheric dilution effects and challenges in definitively attributing measurements to specific sources (Wang et al., 2020b).

In contrast, telematics-integrated on-board diagnostics (OBD) technology enables scalable, real-time collection of vehicle operational and emissions-related parameters directly from the electronic control unit (ECU). This approach offers distinct advantages, including non-intrusive monitoring, continuous data availability, and the capacity to correlate emission anomalies with specific driving patterns and engine operating conditions. Its inherent capability for remote data transmission and fleet-wide scalability makes it particularly suitable for large-scale, continuous compliance monitoring. Consequently, telematics-integrated OBD has emerged as the most viable solution for continuous fleet surveillance (Wang et al., 2022; Zhang et al., 2020).

Building upon this technological foundation, recent research has progressively advanced telematics-based platforms to address real-world NOx monitoring challenges. Wang et al. (2020b) developed a supervisory platform with real-time anomaly detection capabilities, enabling regulatory identification of excessive emitters. Feng et al. (2021) established bus-specific emission factor databases using telematics data, revealing distinct emission patterns across different engine types during urban operations. Concurrently, Ge et al. (2023) pioneered machine learning models for NOx identification, while Ge et al. (2025) validated the 3 B-MAW framework for remote monitoring integration. Despite these significant advances, a critical data quality issue continues to undermine system accuracy and regulatory utility: fundamental reliability concerns in sensor measurements, particularly within retrofitted on-board monitoring (OBM) systems (Zhang et al., 2020).

The most persistent and technically challenging issue affecting data reliability is the NH_3-induced cross-sensitivity during NH_3 slip events, which result from incomplete urea decomposition occurring under transient engine thermal profiles. Crucially, NH_3 triggers electrochemical cross-sensitivity in conventional NOx sensors through catalytic oxidation at electrode surfaces ($4NH_3 + 5O_2 \rightarrow 4NO + 6H_2O$), generating artifactual NOx signals (Zhao et al., 2024). Extensive studies have quantified the severe detrimental impacts of this phenomenon. Funk's assessment reveals that NOx sensors frequently fail to meet the ±20% accuracy requirement under transient conditions, with tailpipe NOx mass error exceeding 50% due to the combined effects of cross-sensitivity and other noise factors (Funk, 2021). During significant NH_3 slip events, particularly those induced by rapid thermal transients, the NOx sensor signal can become dominated by the cross-sensitive NH_3 response, leading to substantial overestimation of actual NOx emissions. Empirical evidence from recent field studies further underscores the pervasiveness and magnitude of this interference. For instance, Yu et al. (2021) demonstrated that Smart Emissions Measurement System (SEMS) equipment, which relies on amperometric NOx sensors, consistently overestimates NOx concentrations compared to PEMS during motorway driving, precisely where urea overdosing and NH_3 slip are most prevalent. Similarly, Jeong et al. (2023) confirmed that NH_3 slip in SCR-equipped vehicles leads to SEMS-measured NOx values exceeding those from PEMS, particularly under high-load conditions where Urea-Water Solution (UWS) injection is maximized. Consequently, this systematic bias not only misrepresents real emissions but also undermines the regulatory utility of low-cost OBM solutions, directly compromising compliance programs by inflating false non-compliance rates and distorting emission inventories, thereby eroding confidence in remote monitoring data and hindering effective air quality management and targeted regulatory enforcement.

To address this challenge, significant research efforts have been directed toward resolving the NH_3 cross-sensitivity problem, primarily through three technical pathways. Physical NH_3 sensor integration has been evaluated by Van Nieuwstadt (Van Nieuwstadt, 2022), who concluded that current NH_3 sensor technology provides limited benefit due to its own tolerance issues, requiring at least twice the current accuracy to yield uniform improvement. Model-based cross-sensitivity compensation approaches have been developed by multiple research groups. Aliramezani et al. (2016) proposed a dynamic NOx/NH_3 cross-sensitivity model coupled with an SCR model, while Childress and Chen (2018) developed a decomposition algorithm for nonlinear systems with cross-sensitive measurements. Jones and Geveci (2011) pioneered smart sensing techniques using Ammonia to NOx Ratio (ANR) perturbation methods to discriminate between NOx and NH_3 components. Additionally, Yan et al. (2019) further optimized urea dosing and NH_3 coverage ratios using NSGA-II algorithms, though such approaches remain computationally intensive for real-time telematics applications. Observer-based state estimation represents a third pathway, where advanced estimation techniques using Extended Kalman Filters (EKF), Square-Root Unscented Kalman Filters (SRUKF), and other observers have been developed to simultaneously estimate SCR aging, urea injection faults, and gas concentrations. Yang et al. (2020) successfully applied SRUKF to estimate NH_3 coverage ratio and input NH_3 concentration, demonstrating improved accuracy over PF and UKF methods.

However, these solutions face fundamental limitations for telematics-based remote monitoring applications. The computational complexity of EKF, SRUKF, and nonlinear decomposition algorithms requires substantial computational resources and high-frequency data processing, which makes large-scale fleet deployment across diverse ECU platforms impractical. Hardware dependency presents another significant barrier, as solutions that rely on additional physical NH_3 sensors face prohibitive cost barriers for retrofit applications while introducing new sources of measurement uncertainty, despite promising advances such as high-accuracy NOx sensors with monitor electrodes developed by Todo et al. (2018). Furthermore, excitation requirements limit practical implementation, as methods utilizing ANR perturbations interfere with normal engine operation and dosing strategies, rendering them unsuitable for continuous monitoring during real-world driving conditions.

Thus, a clear research gap exists in developing a calibration method that is both computationally efficient and hardware-independent. The ideal solution should apply retrospectively to remote data streams without requiring specific vehicle excitation or proprietary ECU integration. This gap is particularly critical for regulatory applications where trustworthy, scalable monitoring solutions are essential for effective compliance verification and data-driven policy refinement across diverse vehicle fleets. To bridge this gap, this study proposes a novel telematics-integrated dual-algorithm framework. The first stage employs a sliding-window detector that adaptively analyzes NH_3 excess index (EI_{NH3}) thresholds to pinpoint NH_3 slip events. The second stage applies a catalyst-state compensation model to correct NOx sensor readings during periods of NH_3 presence. By resolving NH_3-induced

cross-sensitivity at the measurement layer through algorithms suitable for retrospective telematics data processing, the framework bridges the critical gap between emission regulation and real-world enforcement, offering regulators a scientifically robust, scalable methodology for trustworthy remote emission monitoring.

2. Methodology

2.1. Experimental platform and instrumentation

Two China VI-compliant M3 HDDVs (designated as Vehicle A and Vehicle B) were used to quantify NOx sensor deviations against PEMS benchmarks. Two repeat trials were conducted for each vehicle to establish measurement robustness. As detailed in Table 1, both vehicles employed identical aftertreatment architectures, comprising a diesel oxidation catalyst (DOC), a diesel particulate filter (DPF), a copper-modified zeolite-based SCR system, and an ammonia slip catalyst (ASC).

The emissions measurement system integrated two precision instruments, an AVL PEMS 493 for NOx measurement (with a resolution of 5 ppm and sampling at 1 Hz) and a UNISEARCH LasIR laser analyzer for NH_3 quantification (with a resolution of 8 ppm and sampling at 1 Hz) (see Fig. 1). Key performance specifications are summarized in Table 2. All instruments underwent pre-test and post-test calibration following manufacturer protocols, with independent battery power supplies utilized to eliminate electrical interference. The complete measurement setup is illustrated schematically in Fig. 2, which details the sensor placement designed to ensure accurate correlation between sensor readings and reference measurements. A straight extension pipe matching the original exhaust diameter was attached to the tailpipe, with the NOx and NH_3 sampling probes positioned adjacently at the centerline to minimize spatial concentration gradients. Heated PTFE tubing was used for both sample lines to prevent NH_3 adsorption, ensuring that the PEMS and laser analyzer provided reliable benchmark data against which the onboard sensor performance and the proposed correction algorithms could be rigorously evaluated. A venturi flow meter was installed upstream of the sampling points within the extension pipe to measure exhaust flow rate. The entire system was configured for underbody vehicle mounting to minimize aerodynamic effects during on-road operation (see Fig. 3).

2.2. RDE test procedures and data processing

Field testing was conducted on public roads in the temperate plains region of Eastern China, with ambient temperatures maintained between 15 °C and 25 °C, following China VI RDE testing protocols (Yang et al., 2025). Each test trial commenced under cold-start conditions, defined by an engine coolant temperature at or below 30 °C, and continued for approximately 3 h. This duration ensured that the cumulative positive work achieved 4-7 times the reference value of the World Harmonised Transient Cycle (WHTC), a key criterion for data validity stipulated in the regulations (Yang et al., 2025). The driving route was meticulously planned to comprise three distinct phases: urban (accounting for 45 ± 5% of trip duration, average speed 15-30 km/h), rural (25 ± 5%, 45-60 km/h), and motorway (30 ± 5%, >70 km/h), conforming to the stipulated boundaries for trip dynamics (Yang et al., 2025). The resulting speed distribution profiles validate the representativeness of the RDE cycle, showing the required low-speed urban, moderate-speed rural, and sustained high-speed motorway phases. This diversity in driving dynamics is crucial as it induces the transient thermal and load conditions that challenge SCR control and precipitate NH_3 slip, thereby creating the real-world scenarios our method aims to address. Critical operational parameters from the test campaigns are summarized in Table 3.

Table 1
Technical specifications of test vehicles.

Parameter	Vehicle A	Vehicle B
Category	M3	M3
Max. towable mass (kg)	11,850	16,700
Dimensions L × W × H (mm)	8955 × 2346 × 3380	10,990 × 2550 × 3620
Engine displacement	5.1	7.7
Max. power (kW)	169	228
Max. torque (Nm)	940	1400
Emissions standard	China VI	China VI
Aftertreatment system	DOC + DPF + SCR + ASC	DOC + DPF + SCR + ASC

Table 2
Performance specifications of primary measurement instruments.

Parameter	AVL PEMS 393	LasIR Analyzer
Operating temperature range	−30~45 °C	−10~50 °C
Measurement range	0~5000 ppm (NO), 0~2500 ppm (NO_2)	0~1000 ppm (NH_3)
Zero drift	<2 ppm/8 h (NO/NO_2)	<10 ppm/24 h (NH_3)
Power supply	24 V DC	12 V DC
Mass	~50 kg	~5 kg

Following data acquisition, precise temporal synchronization across all measurement streams was achieved by maximizing the Spearman's rank correlation coefficient between paired signals (e.g., vehicle speed from GPS and ECU). This non-parametric method was selected for its robustness to non-linear relationships and outliers. The correlation coefficient (ρ_s) was calculated as:

$$\rho_s = \frac{\frac{1}{n}\sum_{i=1}^{n}(R(x_i)-\overline{R(x)})\cdot(R(y_i)-\overline{R(y)})}{\sqrt{\left(\frac{1}{n}\sum_{i=1}^{n}(R(x_i)-\overline{R(x)})^2\right)\left(\frac{1}{n}\sum_{i=1}^{n}(R(y_i)-\overline{R(y)})^2\right)}} \quad (1)$$

Where $R(x_i)$ and $R(y_i)$ represent the ranks of corresponding data points between two synchronized signals (x, y), respectively. $\overline{R(x)}$ and $\overline{R(y)}$ stand for the mean ranks of x and y, respectively. n is the data length.

Following data acquisition, precise temporal synchronization across all measurement streams was achieved by maximizing the Spearman's rank correlation coefficient between paired signals (e.g., vehicle speed from GPS and ECU). This non-parametric method was selected for its robustness to non-linear relationships and outliers. After optimizing the alignment, the typical residual time-alignment error between the primary signals (e.g., GPS vehicle speed and ECU speed) was estimated to be less than one data sample (i.e., <1 s), ensuring the integrity of all subsequent time-aligned data analysis.

The synchronized NOx and NH_3 concentration profiles from the test (Fig. 4) provide a critical visualization of the core problem. During urban and rural phases, NH_3 levels remain negligible despite fluctuating engine-out NOx, indicating effective storage. However, upon entering the motorway phase, a distinct pattern emerges: sharp rises in NH_3 concentration (exceeding 100 ppm) coincide with periods where the downstream NOx sensor reading diverges positively from the PEMS reference. Under motorway high-speed operation, NH_3 slip deteriorates markedly. This may partly stem from the elevated exhaust mass flow rate at high vehicle speeds, which increases the space velocity and shortens the residence time, thereby imposing more stringent requirements on reductant mixing uniformity. Even minor deviations in the inlet distribution can lead to localized NH_3 overdosage (Birkhold et al., 2007). In addition, the higher exhaust temperature during high-speed driving can rapidly reduce the catalyst NH_3 storage capacity, further exacerbating NH_3 breakthrough (Opitz et al., 2015). Similar NH_3 slip behavior under high-speed, high-load conditions has also been reported by He et al. (2024). As the NH_3 concentration increases, the discrepancy between the NOx sensor signal and the actual NOx

(a) Vehicle A (b) Vehicle B

Fig. 1. Photographs of test vehicles (Category M3).

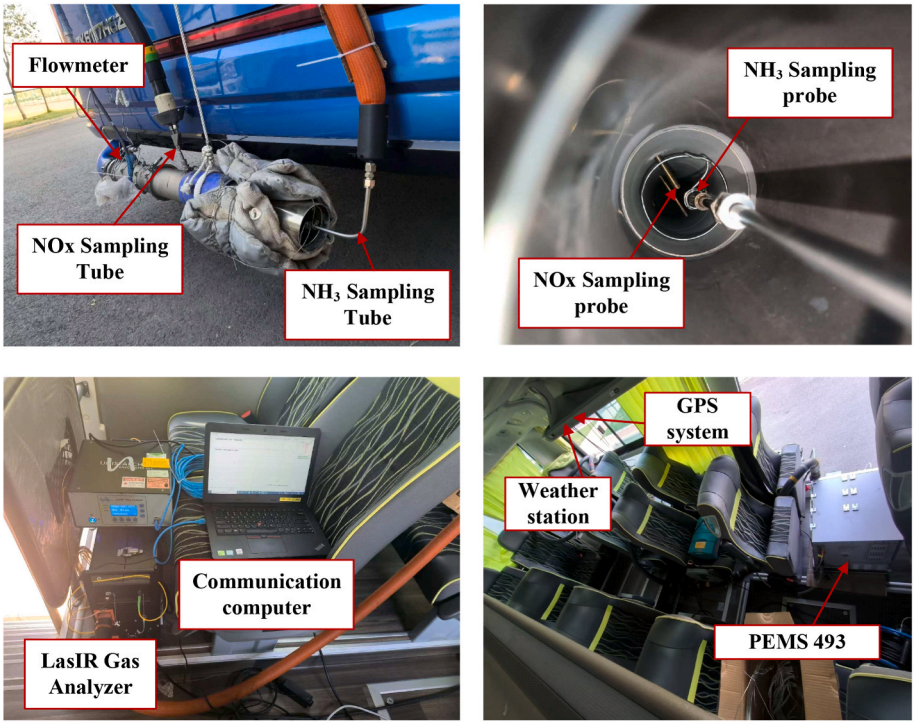

Fig. 2. Schematic of measurement instrumentation and sensor placement.

concentration becomes progressively larger. This inverse correlation provides direct visual evidence of the cross-sensitivity artifact and justifies the need for a phase-aware correction strategy.

NOx compliance was assessed using the Moving Average Window (MAW) method, with the workflow illustrated in Fig. 5. A work-based MAW approach, which normalizes emissions by engine work, forms the basis of regulatory compliance evaluation under China VI. Consecutive windows were initiated once the engine coolant temperature surpassed 70 °C and generated by sliding a window of variable length through the time series. Each window started at a successive time step and ended when the cumulative engine work within that window reached the reference work value (W_{ref}), defined as the total engine work over the WHTC. The specific NOx emissions (SE_{NOx}, in g/kWh) for each window were calculated as:

$$SE_{NOx} = \frac{m_{NOx}}{W_{(t_{2,i})} - W_{(t_{1,i})}} \quad (2)$$

Where m_{NOx} is the total NOx mass per window (g) and $W_{(t_{2,i})} - W_{(t_{1,i})}$ is the corresponding engine work increment over the window (kWh).

The output of this process, specifically the 90th percentile value (SE_{NOx}_P90) of all valid windows, is the key metric our correction framework aims to accurately reproduce. Under the China VI emission standard, a vehicle's real-driving emissions are deemed compliant if its SE_{NOx}_P90 remains below the regulatory limit of 0.69 g/kWh. This metric is also consistent with the Euro VI and upcoming Euro VII approaches, making it internationally relevant. Concurrently, the average power within each window was calculated as a ratio relative to the maximum engine power. For a test to be considered valid, three critical criteria had to be satisfied: an initial power threshold of at least 20% of maximum engine power, a minimum of 50% valid windows across the entire driving cycle, and adherence to an absolute minimum power threshold of 10% throughout the entire operating period. Tests failing to maintain the 10% minimum power threshold at any point were classified as non-compliant.

2.3. NH_3 slip identification and data correction

2.3.1. Acquisition of Urea-Water Solution dosing data

NH_3 slip primarily results from two mechanisms: physical

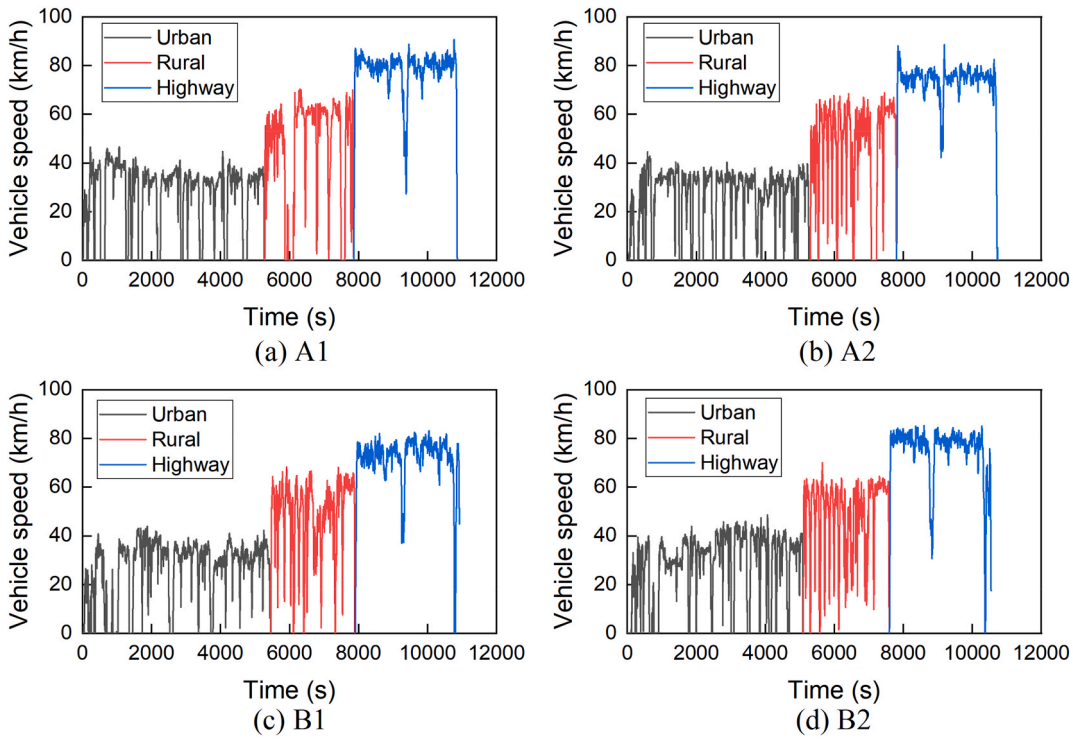

Fig. 3. Vehicle speed distribution profiles across urban, rural, and motorway phases.

Table 3
Operational parameters of RDE test campaigns.

Parameter	A1	A2	B1	B2
Duration (s)	10,872	10,743	10,930	10,545
Urban phase (%)	45.6	46.3	47.0	45.2
Rural phase (%)	25.1	24.7	23.7	25.1
Highway phase (%)	29.3	29.0	29.2	29.7
Urban mean speed (km/h)	27.4	25.4	26.5	27.9
Rural mean speed (km/h)	45.9	46.7	48.1	48.1
Highway mean speed (km/h)	77.8	72.9	71.5	74.6

breakthrough of unabsorbed NH_3 through catalyst channels, and desorption of stored NH_3 due to sudden changes in operating conditions. Under modern SCR catalyst designs, a physical breakthrough occurs infrequently. Thus, the direct cause of NH_3 slip is typically the desorption of stored NH_3 triggered by transient operations, while the root cause is prior excess NH_3 supply. Consequently, identifying an oversupply of NH_3 constitutes a crucial prerequisite for detecting NH_3 slip. Accurately quantifying the UWS injection amount is critical, as it plays a vital role in regulating NH_3 generation. However, this parameter is not a mandatory upload requirement to the remote monitoring system. To address this data gap, a predictive model for UWS injection rate was developed, integrating multidimensional operational parameters (e.g., engine speed, torque) with emission control variables (e.g., SCR temperature,

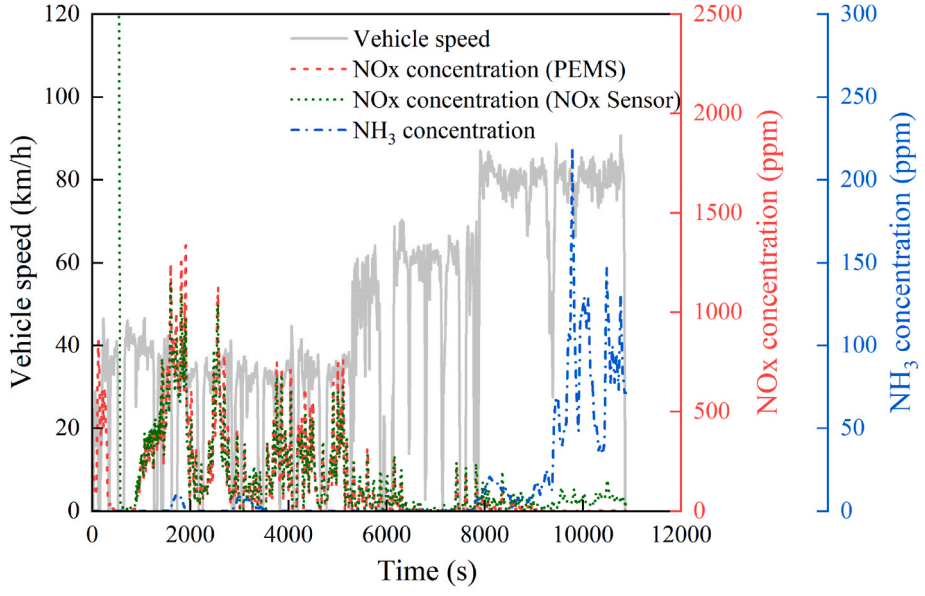

Fig. 4. Synchronized NOx-NH_3 concentration profiles across driving phases for the test.

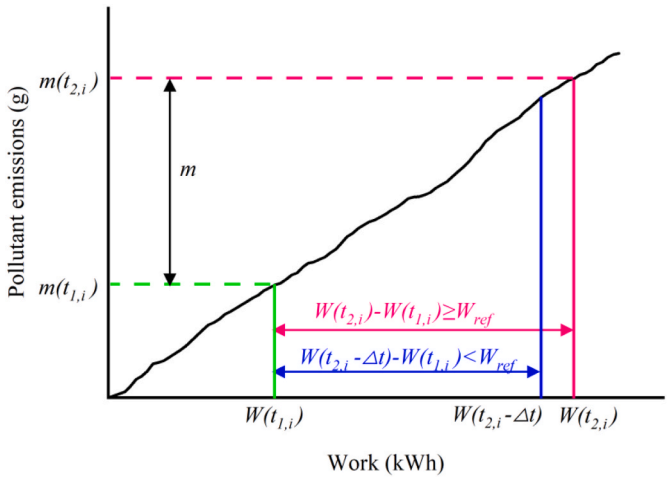

Fig. 5. Workflow of the MAW method for compliance assessment.

NOx sensor readings).

Vehicle remote monitoring data collected over one month of normal on-road operation of vehicles A and B was utilized as the training dataset. To calibrate the UWS injection rate, a data acquisition and transmission device was installed on the test vehicles, specifically designed to obtain the actual UWS injection rate from the ECU. The UWS initiation temperature for each vehicle was empirically determined by analyzing the recorded SCR inlet temperature at the moment the ECU first commanded a non-zero UWS injection during the engine warm-up phase across multiple test cycles. Statistical analysis in Fig. 6 revealed that the UWS initiation temperature differed between the two test vehicles: 185 °C for Vehicle A and 190 °C for Vehicle B, measured at the SCR system inlet. Subsequent consultation with the manufacturers confirmed that these values align with their proprietary urea dosing calibration, indicating that the method can accurately determine the initiation temperature. The relationship between SCR inlet temperature and urea dosing confirms the existence of a vehicle-specific temperature threshold for dosing activation. More importantly, it shows that above this threshold, the dosing rate is highly variable and poorly correlated with temperature alone, justifying the need for a multi-parameter predictive model that captures the influence of engine operation and NOx production. To enhance training efficiency, only data where the SCR system inlet temperature exceeded the respective vehicle's UWS initiation temperature were used for model training.

Parameter selection for the predictive model involved systematic elimination of non-essential variables (e.g., reagent residue, fuel tank level) and incorporation of key NOx control parameters including excess air coefficient (λ), space velocity (SV), and upstream NOx mass flow rate ($\dot{m}_{NOx\_up}$) (calculated per Eqs. (3)–(5)):

$$\lambda = \frac{\dot{m}_{air}}{\dot{m}_{fuel} \times 14.3} \tag{3}$$

$$SV = \frac{\dot{m}_{exh} \times R \times T_{cat}}{P \times V_{SCR} \times M_{exh}} \tag{4}$$

$$\dot{m}_{NOx\_up} = \frac{c_{NOx\_up} \times 10^{-6} \times \dot{m}_{exh} \times \frac{1000}{3600} \times M_{NOx}}{22.4 \times 10^{-3} \times \rho \times 10^{3}} = 4.412 \times 10^{-7} \times c_{NOx\_up} \times \dot{m}_{exh} \tag{5}$$

Where, $\dot{m}_{air}$ denotes the intake mass flow rate (kg/h), $\dot{m}_{fuel}$ denotes the fuel flow rate (kg/h), $\dot{m}_{exh}$ denotes the exhaust flow rate (kg/h). R is the universal gas constant (8.314 J/mol·K), T_{cat} denotes the SCR catalyst temperature (K), P denotes the exhaust pressure (Pa). V_{SCR} denotes the geometry volume of the SCR system (m^3), which is a manufacturer-specified parameter and obtained from the vehicle's technical documentation. M_{exh} denotes the exhaust molar mass (g/mol), c_{NOx_up} denotes the SCR upstream NOx concentration (ppm). To ensure consistency with emission regulatory requirements, the NO_2-equivalent molar mass of NOx (M_{NOx} = 46 g/mol) was adopted in all calculations, and the exhaust gas density ρ was approximated by the standard air density (1.293 kg/m^3).

Time-series analysis was necessary due to the nonlinear dynamics of the SCR system, particularly the time-delayed responses in NH_3 storage. Through Spearman's rank correlation analysis, a set of 13 core input parameters were identified for the prediction model, including vehicle speed, net engine torque, friction torque, engine speed, fuel flow rate, air flow rate, SCR system inlet temperature, SCR system outlet temperature, engine coolant temperature, SCR upstream NOx sensor readings, λ, SV and $\dot{m}_{NOx\_up}$. Fig. 7 provides a quantitative rationale for feature selection, showing strong positive correlations between UWS injection rate and parameters directly related to engine load and NOx production (net engine torque, engine speed, fuel flow rate, air flow rate, SCR upstream NOx sensor readings, λ, SV and $\dot{m}_{NOx\_up}$). This analysis solidified the choice of input parameters for the prediction model, ensuring it focuses on the most influential variables. Parameters showing weak association, such as barometric pressure ($\rho_s < 0.05$), were excluded.

Although the dynamic NH_3 storage level within the SCR system cannot be directly measured by any sensor (Childress and Chen, 2018), its trend can be inferred indirectly by analyzing the supply and

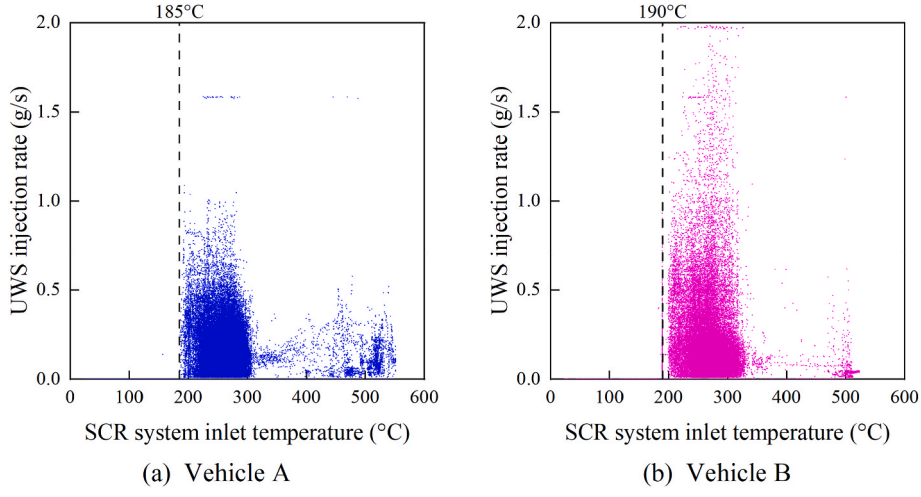

Fig. 6. SCR inlet temperature versus UWS injection rate for Vehicles A and B.

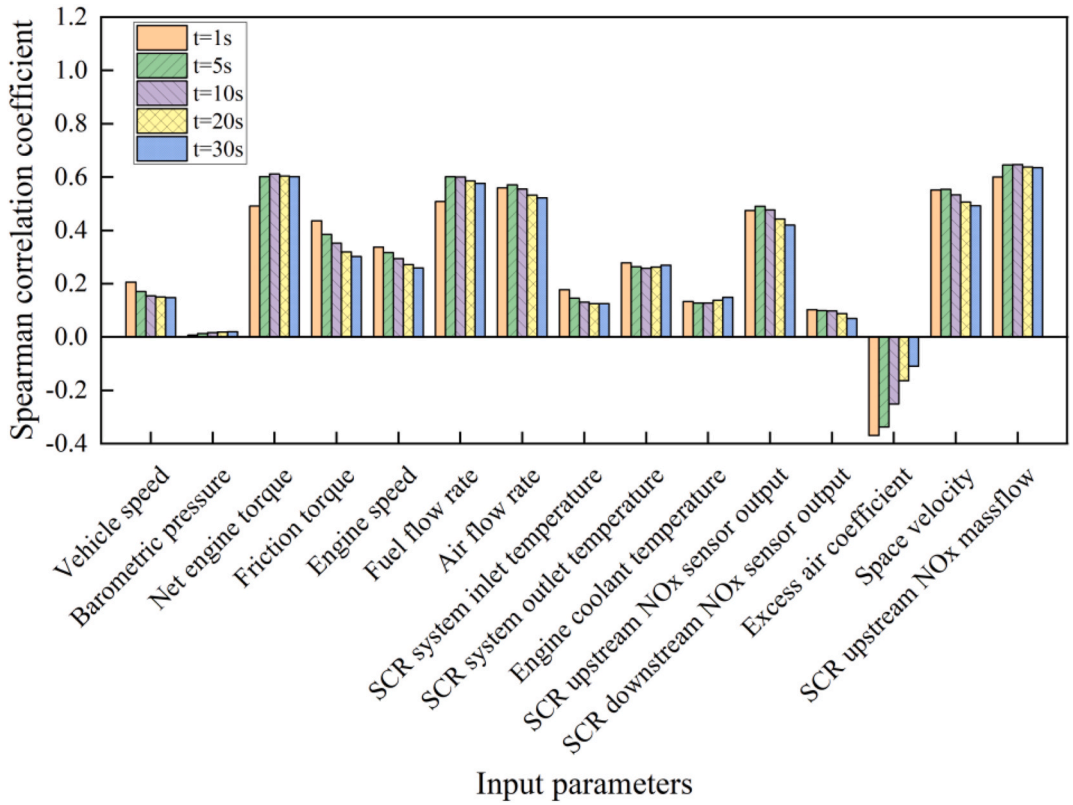

Fig. 7. Spearman correlation analysis between input parameters and UWS injection rate.

consumption of NH_3 over a specific period. An increase in the upstream NOx mass flow rate promotes higher NH_3 consumption, leading to decreased NH_3 storage levels. To replenish the consumed NH_3, the UWS injection rate is adjusted accordingly. Therefore, to predict the UWS injection rate, a Long Short-Term Memory (LSTM) regression algorithm was selected. The key advantage of using an LSTM for this task is its ability to implicitly learn and represent dynamic system states, such as the NH_3 storage level, without requiring an explicit assumption about the initial storage. The LSTM's memory cells retain information from previous time steps, capturing temporal dependencies inherent in the SCR system. The model learns the complex, non-linear dynamics, including the effects of NH_3 slip, directly from the time-series data of input parameters and the target UWS injection rate. Consequently, an explicit assumption about the initial NH_3 storage state is not required; the model's internal state is initialized and updated based on the sequence of preceding data points, effectively capturing the supply–consumption–storage–slip balance over time. The LSTM model was constructed with two hidden layers. To preserve data sequence continuity, 80% of the experimental data was used for training, and the remaining 20% was reserved for testing. The model was optimized by minimizing the Mean Squared Error (MSE) on the validation set, tuning the memory window length and the number of nodes in the hidden layers. The final optimized LSTM model utilized a memory window of 60 s and hidden layers with 40 and 60 nodes, respectively.

The model's performance on the test set demonstrated close agreement between predicted and measured injection rates, with minor local discrepancies attributable to limitations in the telematics data acquisition system, as shown in Fig. 8. On the held-out test set, the LSTM model achieved a Root Mean Square Error (RMSE) of 0.0867 and a Mean Absolute Error (MAE) of 0.0518 for the normalized instantaneous UWS injection rate prediction for Vehicle A, and correspondingly 0.1099 and 0.0588 for Vehicle B. The slightly higher RMSE for Vehicle B reflects the more challenging transient dosing patterns observed in that vehicle, but it remains well within acceptable limits. Crucially, the prediction of cumulative UWS mass, particularly valuable for NH_3 slip identification compared to instantaneous rate monitoring, maintained an error within ±10% (Vehicle A: 5.0%; Vehicle B: 8.7%), as shown in Fig. 9. These results validate the LSTM model as an effective "virtual sensor" for UWS dosing. Fig. 8 shows good tracking of transient injection patterns, while Fig. 9 demonstrates that any instantaneous errors do not accumulate seriously, resulting in highly accurate cumulative mass prediction. This cumulative accuracy is paramount for reliably calculating the NH_3 Excess Index in the next step.

2.3.2. *Determination of the NH_3 excess index*

Following the acquisition of NH_3 supply data, confirming whether excess NH_3 supply has occurred is essential. To quantify the degree of NH_3 surplus, this study proposes the NH_3 Excess Index (EI_{NH3}). The calculation procedure is described below.

NH_3 is derived from urea (NH_2CONH_2) in the UWS via thermal decomposition. Standard UWS has a urea concentration of 32.5% (Hu et al., 2011). Assuming complete conversion of urea to NH_3, the mass ratio of UWS to released NH_3 can be determined from their molar masses:

$$\frac{m_{UWS}}{m_{NH_3}} = \frac{60/0.325}{17 \times 2} \approx 5.43 \tag{6}$$

Where m_{UWS} is the mass of the UWS (g) and m_{NH_3} is the mass of NH_3 released (g)

Based on the stoichiometric reaction between NH_3 and NOx and their molar masses, the mass ratio of NH_3 to NOx is:

$$\frac{m_{NH_3}}{m_{NO_x}} = \frac{17}{46} \approx 0.37 \tag{7}$$

Where m_{NOx} is the mass of NOx (g).

Consequently, the theoretical mass ratio of UWS to NOx is:

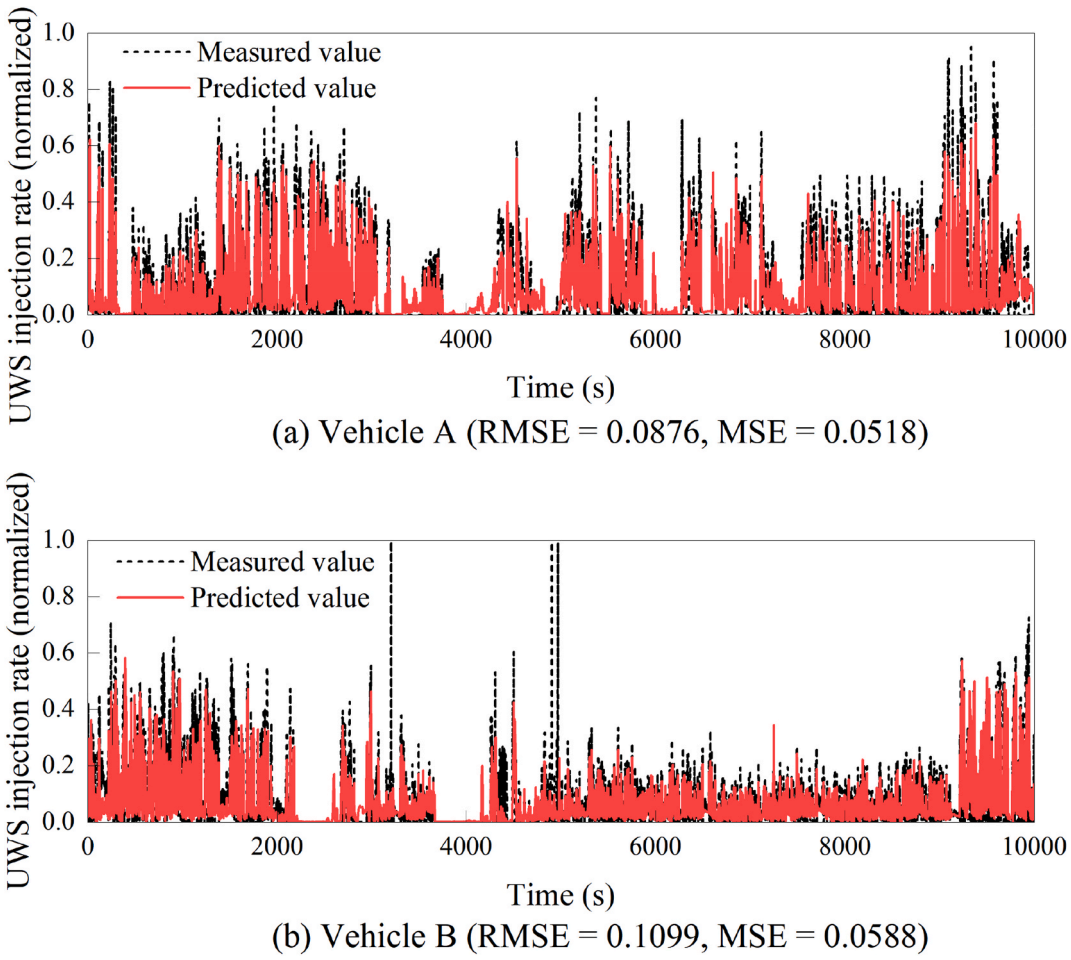

Fig. 8. Time-series comparison of predicted vs. measured UWS injection rate (The first 10,000 s).

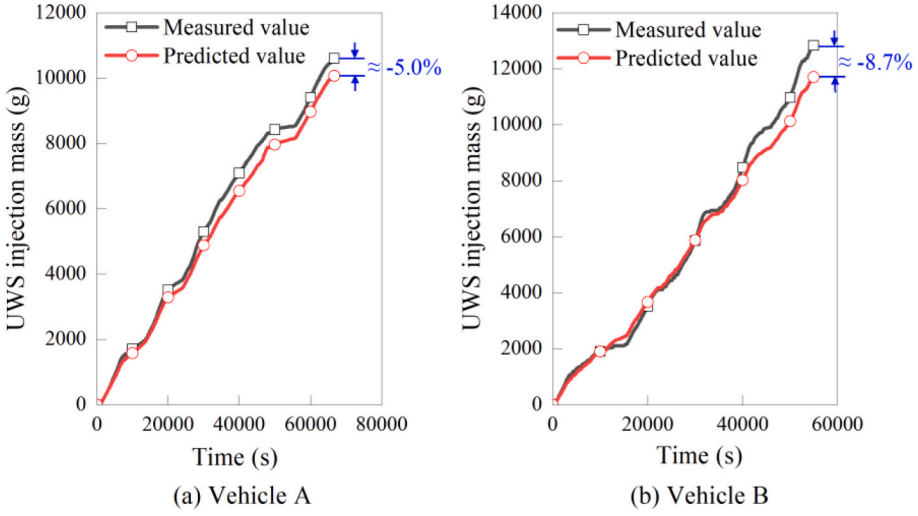

Fig. 9. Cumulative UWS mass prediction accuracy over the entire test.

$$\frac{m_{UWS}}{m_{NO_x}} = 5.43 \times 0.37 \approx 2.01 \quad (8)$$

The EI_{NH3} is then defined as:

$$EI_{NH_3} = \frac{m_{UWS} - m_{NOx\_up} \times 2.01}{5.43 \times V_{SCR}} \quad (9)$$

Where m_{NOx_up} is the mass of upstream NOx (g) and V_{SCR} is the volume of the SCR system (L). The denominator ($5.43 \times V_{SCR}$) serves to normalize the excess NH_3 mass by the SCR volume, yielding a quantity with units of g/L that reflects the degree of NH_3 surplus per unit catalyst volume. A value of $EI_{NH3} > 0$ indicates that the cumulative NH_3 supply has exceeded the stoichiometric demand for reducing the SCR upstream

NOx mass, implying a potential for NH_3 slip.

2.3.3. Identification of NH_3 slip

The NH_3 slip diagnostic protocol was developed through systematic integration of EI_{NH3} with the observed SCR conversion efficiency, as illustrated in the decision flowchart in Fig. 10. The logic encapsulated in Fig. 10 is central to the identification algorithm. It moves beyond simple thresholding on a single parameter. Instead, it interprets the concurrent state of two indicators: the supply-demand balance (EI_{NH3}) and the system's effectiveness (observed SCR efficiency). A slip is flagged only when excess EI_{NH3} is supplied ($EI_{NH3} > 0$) and the system efficiency drops (e.g., <98%), indicating that the excess EI_{NH3} is not being utilized for NOx reduction and is therefore slipping. This dual-condition check significantly improves discrimination against false positives. When the SCR system operates within its optimal temperature window (220-500 °C) (Yan et al., 2019; Feng and Lu, 2015; Zhao et al., 2011), two distinct behavioral modes are identified.

(1) NOx-dominated exhaust regime (indicating low NH_3 storage capacity on the catalyst)

For $EI_{NH3} > 0$, a progressive increase in NH_3 surface coverage enhances the actual SCR conversion efficiency. For $EI_{NH3} < 0$, declining NH_3 coverage reduces catalytic activity and the actual SCR conversion efficiency.

(2) NH_3-dominated exhaust regime (indicating approaching or saturated NH_3 storage)

For $EI_{NH3} > 0$, excessive NH_3 supply leads to slip events and reduced observed SCR conversion efficiency. For $EI_{NH3} < 0$, controlled NH_3 injection mitigates slip risk while helping to restore conversion efficiency.

To address potential inaccuracies in the predicted UWS injection rate and accommodate the SCR system's inherent response delays, the diagnostic implementation employs a 10-s observation window. This duration provides sufficient stability for capturing system dynamics and NH_3 storage variations while maintaining responsiveness to transient conditions. Furthermore, the protocol requires two consecutive positive detections within these observation windows to confirm a slip event, significantly enhancing robustness against false positives. A slip condition is automatically reset when EI_{NH3} falls below 0 concurrently with the observed SCR efficiency exceeding 98%, creating a dual-threshold approach that effectively balances detection sensitivity with operational reliability across diverse driving conditions.

2.3.4. Correction of NOx sensor measurements during NH_3 slip

The upstream NOx sensor, unaffected by NH_3 slip, generally delivers highly accurate measurements and can serve as a reliable reference. The downstream NOx sensor also provides reliable readings under NH_3-free conditions. However, during NH_3 slip events, the sensor error is dominated by cross-sensitivity effects, rendering its direct NOx measurements unreliable. NH_3 slip typically occurs when the NH_3 supply exceeds the saturated NH_3 storage capacity of the catalyst (Hu et al., 2011). Fig. 11 illustrates the relationship between NH_3 concentration and SCR system temperature. Given that the measurement precision of the NH_3 analyzer is 8 ppm, 20 ppm was preliminarily established as the threshold for significant NH_3 slip. It is evident that significant NH_3 slip (>20 ppm) occurs almost exclusively at SCR system temperatures above 220 °C, where the exhaust composition shifts to an NH_3-dominated state, with only trace levels of residual NOx present. This establishes a crucial empirical boundary for applying the correction. Therefore, the correction is only applied when two conditions are met: 1) a slip event is identified via Fig. 10 logic, and 2) the SCR temperature is above 220 °C. This prevents unnecessary correction during low-temperature operation.

PEMS measurements under these specific conditions reveal that tailpipe NOx concentrations approach instrumental detection limits, while the calculated SCR conversion efficiency consistently surpasses 99%, as shown in Fig. 12. The box plot provides the empirical justification for the fixed 99% efficiency assumption. During significant slip,

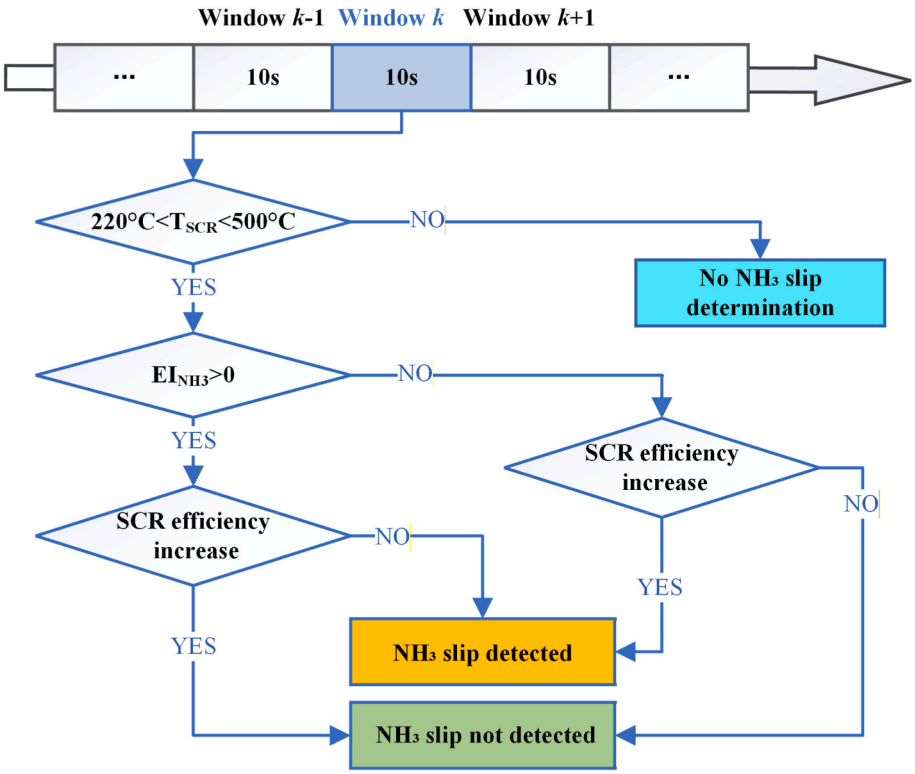

Fig. 10. Decision flowchart integrating EI_{NH_3} and SCR efficiency.

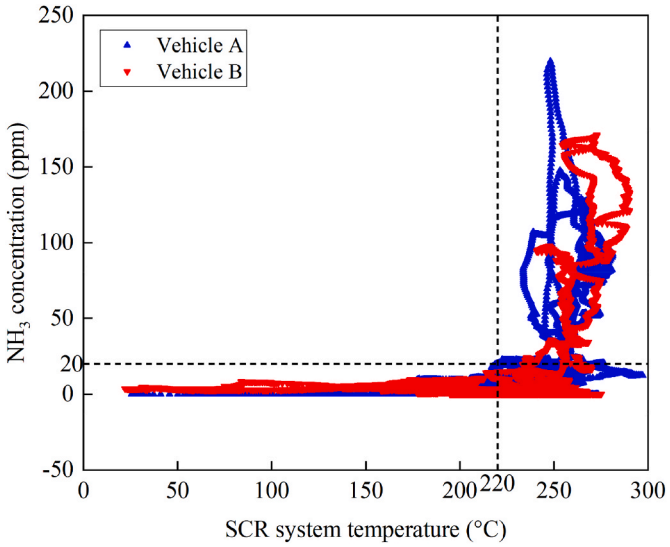

Fig. 11. Relationship between NH_3 slip concentration and SCR system temperature.

the actual SCR efficiency measured by PEMS is overwhelmingly high (>99%). This key observation allows for a drastic simplification: instead of trying to model the complex cross-sensitivity or estimate the precise slip concentration, we assume that when NH_3 is slipping, the catalyst is still highly effective, and the true tailpipe NOx is merely 1% of the engine-out NOx. This simplification is the cornerstone of the method's practicality for fleet-wide telematics processing. Given that upstream NOx concentrations in these scenarios typically remain below 2000 ppm, the theoretical downstream NOx concentration at 99% conversion efficiency would be below 20 ppm, a range comparable to the precision limits of commercial NOx sensors. This mechanistic understanding underpins our proposed correction method, which is under confirmed NH_3 slip conditions, a fixed 99% conversion efficiency is applied to estimate the actual downstream NOx concentration, as calculated by Eq. (10). This approach provides a physically plausible and conservative estimate of NOx emissions when the direct sensor reading is compromised by significant NH_3 interference.

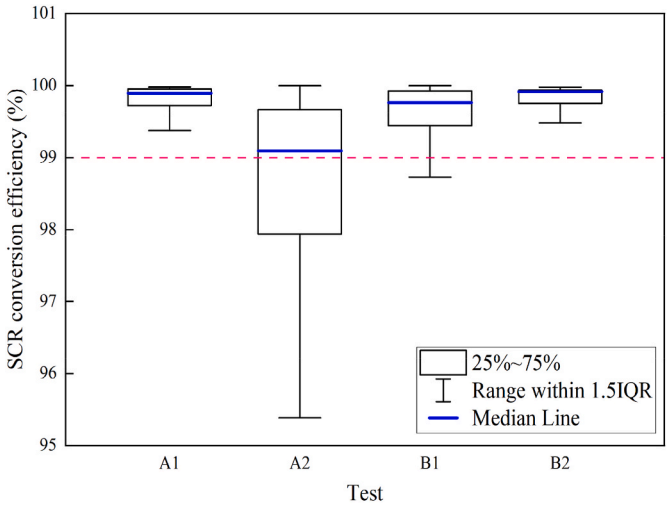

Note: The IQR (Interquartile Range) represents the range of the middle 50% of data points in a distribution, calculated as the difference between the 75th percentile and the 25th percentile.

Fig. 12. Distribution of actual SCR efficiency during NH_3 slip periods (>20 ppm).

$$c_{NOx\_down\_cor} = c_{NOx\_up} \times (1\text{-}0.99) \quad (10)$$

Where $c_{NOx\_down\_cor}$ denotes the corrected SCR downstream NOx concentration (ppm).

3. Results

3.1. NH_3 slip identification

A binary classification framework based on a confusion matrix was constructed to evaluate the performance of the NH_3 slip detection methodology, as shown in Table 4. Using 10-s evaluation windows, comparisons between model predictions and measured results were classified into four categories: True Positives (TP) represents correctly identified NH_3 slip events. False Positives (FP) indicates false alarms. False Negatives (FN) corresponds to undetected NH_3 slip events. True Negatives (TN) denotes correctly identified non-slip periods. The regulatory implications of classification errors warrant careful consideration. Missed events (FN) lead to an overestimation of NOx emissions, potentially misclassifying compliant vehicles as non-compliant, thereby affecting the fairness of remote monitoring programs. FP, i.e., unnecessary corrections, may slightly underestimate true NOx emissions, potentially masking actual exceedances. From a regulatory perspective, FPs are a less critical issue than FNs because they introduce only a minor leniency bias. To determine the occurrence of NH_3 slip based on experimental results, a threshold of 20 ppm was preliminarily established as the criterion for significant NH_3 slip.

Model performance was quantitatively assessed using three key metrics: Precision, Recall, and Accuracy, calculated via Eqs. (11)–(13). These metrics respectively evaluate the reliability of positive predictions (Precision), the completeness of actual slip event detection (Recall), and the overall classification correctness (Accuracy).

$$\text{Precision} = \frac{TP}{TP + FP} \quad (11)$$

$$\text{Recall} = \frac{TP}{TP + FN} \quad (12)$$

$$\text{Accuracy} = \frac{TP + TN}{TP + FP + FN + TN} \quad (13)$$

Analysis across four independent RDE tests demonstrates robust performance of the method, with Recall values ranging from 77% to 97%, as shown in Fig. 13(a). This confirms that the method successfully identifies the vast majority of actual NH_3 slip events. In all tests, Precision exceeded 75%, indicating that most positive predictions correspond to genuine slip events. Overall accuracy remained above 93% under all conditions, verifying the robustness of the method under real-world driving scenarios. The performance metrics presented in Fig. 13 (a) demonstrate the effectiveness of the identification algorithm. The high Recall (77-97%) is particularly important for a compliance-oriented tool, as it minimizes the risk of missing actual slip events that cause measurement bias. The variable Recall between tests may reflect different slip characteristics or more challenging transient conditions. Precision above 75% indicates an acceptable false alarm rate, and the consistently high accuracy (>93%) confirms the method's overall reliability for distinguishing slip from non-slip conditions. Furthermore, the sensitivity of the NH_3 slip identification algorithm to the NH_3 slip

Table 4
Confusion matrix for binary classification.

Measured result	Predicted result	
	NH_3 slip	No NH_3 slip
NH_3 slip	TP	FN
No NH_3 slip	FP	TN

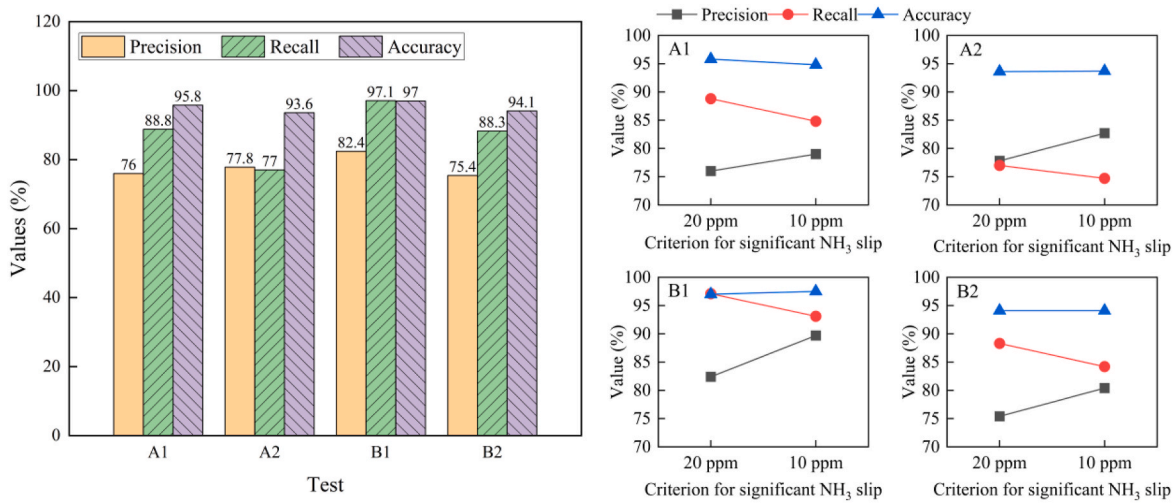

(a) Performance comparison with threshold of 20 ppm (b) Performance variation with different thresholds

Fig. 13. Performance metrics distribution across test cycles.

threshold was analyzed by varying this threshold. When the threshold was reduced to 10 ppm, the measured instances of NH_3 slip increased. However, the algorithm failed to identify all of them, resulting in a slight decrease in Recall (an average reduction of 3.6% across four tests). Concurrently, the Precision of the algorithm improved (an average increase of 5.1% across four tests), indicating a reduced risk of misclassification. Overall, the accuracy of the NH_3 slip identification algorithm remained largely unchanged, with a maximum variation of 1%. This demonstrates that the algorithm is insensitive to changes in the NH_3 slip threshold, exhibiting high robustness.

Given that the measurement of UWS-related signals in remote monitoring data may involve a certain degree of uncertainty, random errors within ±5% and ±10% were artificially introduced into the input parameters of the LSTM model to simulate this measurement uncertainty. The impact of these errors on the prediction of UWS cumulative mass and the performance of NH_3 slip detection was then examined. Taking test A1 as an example, the changes in UWS cumulative mass prediction error and NH_3 slip detection performance after introducing random errors are presented in Table 5. After introducing random errors of ±5%, the UWS cumulative mass prediction error increased slightly (from −5.0% to −6.1%). However, when the random error was further increased to ±10%, the prediction error decreased slightly (from −5.0% to −4.8%). This indicates that the UWS cumulative mass prediction error is highly robust to random errors in the LSTM model input parameters. Regarding NH_3 slip detection performance, the introduction of random errors led to a decrease in Recall, Precision, and Accuracy. At a random error level of ±5%, the Recall, Precision, and Accuracy decreased by 2.7%, 4.5%, and 2.4%, respectively, all within 5%. At a random error level of ±10%, the Recall, Precision, and Accuracy decreased by 6.3%, 9%, and 4.6%, respectively, all below 10%. Overall, the Recall, Precision, and Accuracy of NH_3 slip identification also demonstrate high robustness to UWS prediction uncertainty. This robustness can be attributed to two factors: (1) the cumulative calculation of EI_{NH3} smooths out instantaneous prediction errors, and (2) the dual-condition detection logic ($EI_{NH3} > 0$ and a decrease in SCR efficiency) buffers a certain degree of inaccuracy."

Table 5
Effects of random errors in input data on UWS prediction and NH_3 slip detection performance for test A1.

Items	Values		
Random error level	0 (Raw data)	±5%	±10 %
UWS cumulative mass prediction error	−5.0%	−6.1%	−4.8%
Recall for NH_3 slip identification	76%	73.3%	69.7%
Precision for NH_3 slip identification	88.8%	84.3%	79.8%
Accuracy for NH_3 slip identification	95.8%	93.4%	91.2%

3.2. NOx sensor measurement correction results

The effectiveness of the proposed NOx correction method during NH_3 slip events was evaluated through a comparative analysis against PEMS benchmark data. Fig. 14 presents the telematically monitored raw NOx emissions, the corrected NOx values obtained by applying the proposed method, and the corresponding PEMS-measured reference NOx values across different driving cycles. These plots provide direct visual evidence of the correction's impact. The raw NOx sensor signals show characteristic spikes during motorway driving that are completely absent in the PEMS reference. These spikes are unequivocally identified as NH_3 cross-sensitivity artifacts. The corrected signals closely track the PEMS baseline, effectively eliminating the spurious spikes caused by NH_3 interference. The magnitude of the residual error after post-correction decreased significantly. Due to variations in vehicle speed and acceleration, the four cycles exhibit distinct NOx emission characteristics. Taking the A1 test cycle as an example, a pronounced deviation between the raw emissions and the PEMS reference was observed between approximately 8000 and 9000 s and after 10,000 s, resulting in a RMSE of 52 ppm for NOx concentration data where the SCR temperature exceeded 220 °C. After applying the correction method, the RMSE between the corrected values and the PEMS reference was reduced to 26 ppm. Similarly, following correction, the RMSE for the A2 cycle decreased from 50 ppm to 35 ppm, for the B1 cycle from 133 ppm to 55 ppm, and for the B2 cycle from 66 ppm to 39 ppm. The B1 case exhibits the largest initial RMSE and the greatest absolute improvement, highlighting the method's value in scenarios with severe interference. This consistent performance across diverse cycles confirms the algorithm's robustness in real-world conditions.

3.3. NOx emission compliance assessment results

The ultimate test of the framework's utility is its impact on the regulatory compliance metric, SE_{NOx}_P90. To assess the generalizability of the proposed method, this study conducted RDE tests on China VI HDDVs with multiple categories, including two category N2 vehicles (Vehicles C and D), two category N3 vehicles (Vehicles E and F), and a

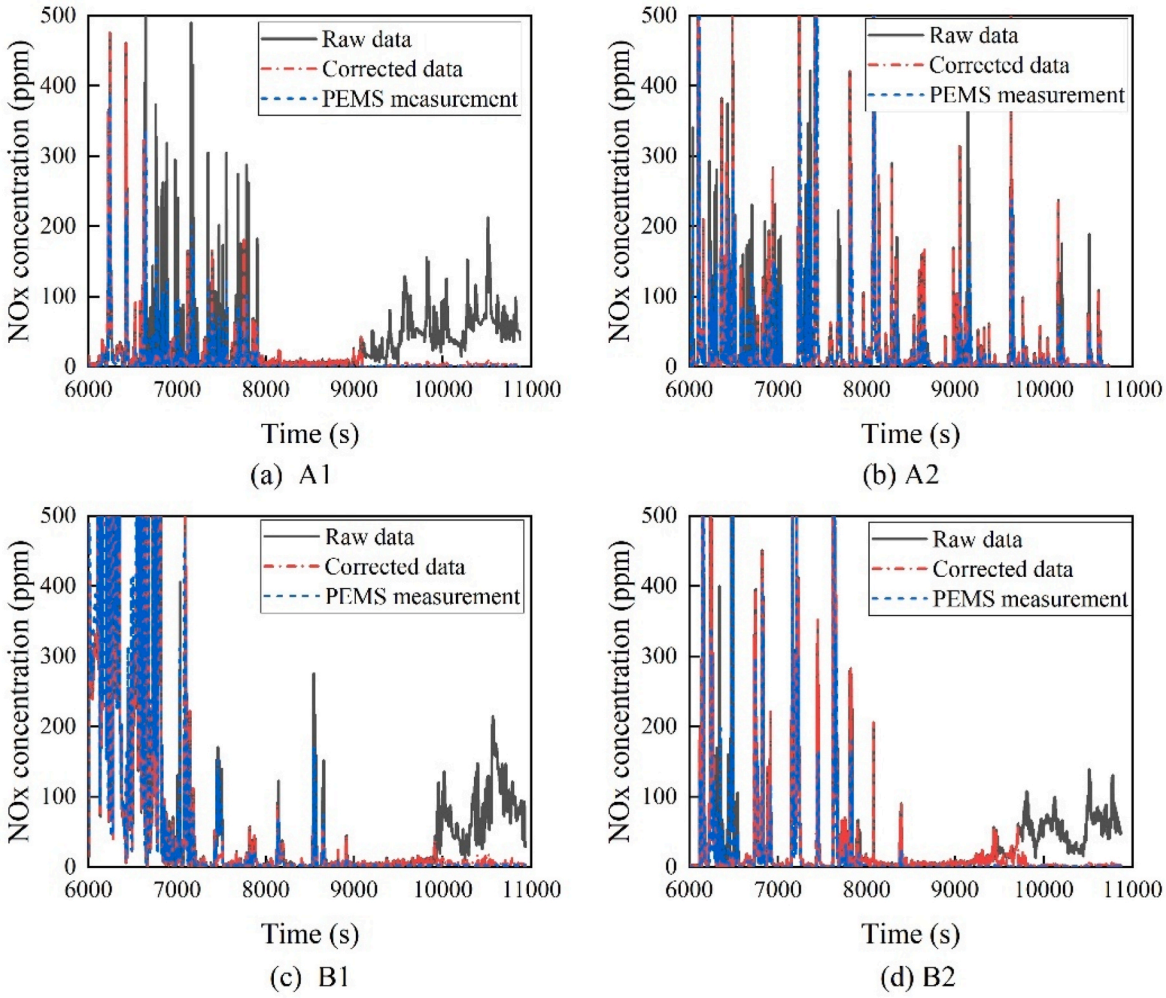

Fig. 14. Time-series comparison of raw, corrected, and PEMS-measured NOx concentrations for the RDE tests.

category M3 vehicle (Vehicle G). Each vehicle underwent two test trials, and NOx emissions before and after correction were compared. Fig. 15 presents the most consequential result for regulatory application. By comparing the raw data, corrected data, and PEMS measurement data, it can be observed that, after applying the correction algorithm, all tested vehicle configurations exhibited a systematic reduction in their

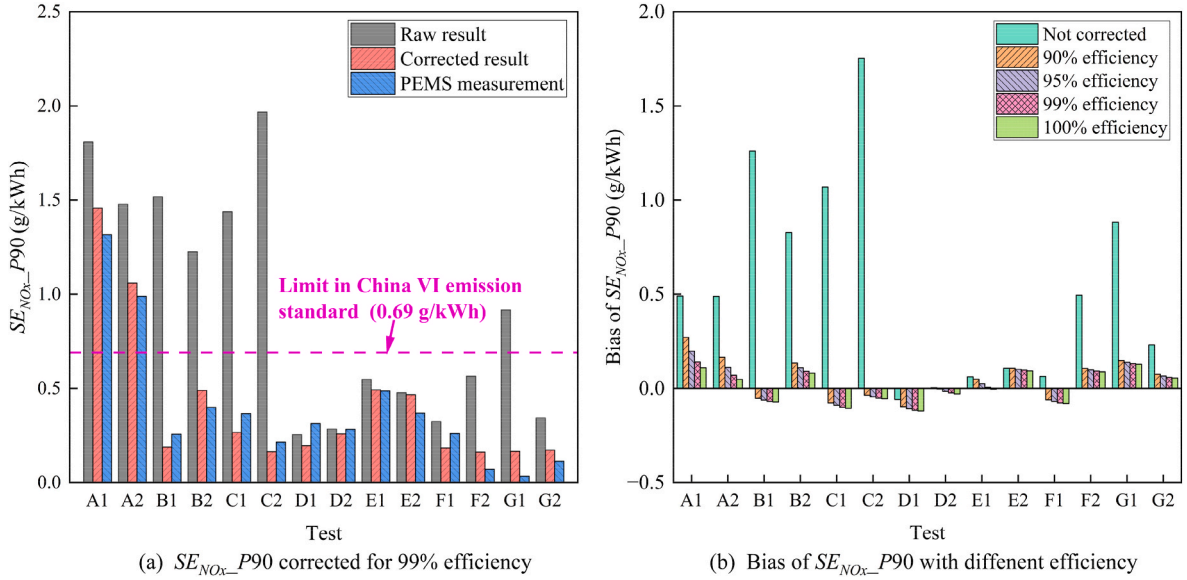

Fig. 15. Comparison of SE_{NOx}_P90 values before and after correction for all test runs.

calculated SE_{NOx}_P90. The absolute error distribution between the corrected data and the PEMS benchmarks was calculated. The mean absolute error decreased from 0.50 g/kWh to 0.03 g/kWh, representing a 94% reduction. Notably, five test runs (B1, B2, C1, C2, G1) would have been falsely flagged as non-compliant based on raw sensor data. After applying the corrected method, all their SE_{NOx}_P90 values fall below the 0.69 g/kWh limit. Taking Vehicle B as an illustrative case (tests B1 and B2), the correction method effectively suppresses spurious NOx signals in the raw data caused by severe NH_3 slip during the highway phase (Fig. 14(c) and d). This directly reduces false non-compliance rates, preventing unjustified penalties and improving the fairness of remote monitoring programs. To assess the impact of the assumed SCR efficiency on the corrected SE_{NOx}_P90, a sensitivity analysis was conducted. Correction coefficients corresponding to efficiencies of 90%, 95%, 99% (baseline), and 100% were applied to the identified slip events. To assess the impact of the assumed SCR efficiency on the corrected SE_{NOx}_P90, a sensitivity analysis was conducted. Correction coefficients corresponding to efficiencies of 90%, 95%, 99% (baseline), and 100% were applied to the identified slip events. The results show that the corrected SE_{NOx}_P90 value decreases as the assumed SCR efficiency increases. Critically, the variation between the values obtained with 95%, 99%, and 100% efficiency is minimal (less than 0.06 g/kWh). This indicates that the final compliance assessment is not highly sensitive to the exact efficiency value within this plausible range around 99%. Even under the most conservative assumption of 90% efficiency, the corrected value deviates from the PEMS benchmark by only 0.27 g/kWh, which is still far below the regulatory limit of 0.69 g/kWh.

Catalyst aging typically reduces NH_3 storage capacity and NOx conversion efficiency. NH_3 slip may occur on aged catalysts at lower efficiency values. For severely aged catalysts, the actual SCR efficiency during slip events could potentially fall below 90%. Future work should incorporate catalyst aging models to dynamically adjust the baseline efficiency based on vehicle mileage or estimated SCR performance degradation.

Fig. 16 further evaluates the consistency between vehicle-level SE_{NOx}_P90 values before and after NH_3-slip correction, and the actual values measured by PEMS. Aggregating results from seven vehicles over 14 RDE trips shows that the uncorrected values exhibit a pronounced systematic bias and substantial dispersion (fitted relationship: $y = 0.58075x+0.77448$), indicating that NH_3 slip can induce significant measurement artifacts with no consistent or stable trend across vehicles and trips. Moreover, the corrected data cluster tightly around the 1:1 relationship, the regression slope is 0.96497, approaching the ideal value of 1, and the intercept is 0.03657 g/kWh, approaching 0. These results indicate that the proposed correction effectively removes the systematic NH_3-induced artifact and restores the baseline accuracy required for OBM-based remote monitoring to serve as a trustworthy regulatory instrument.

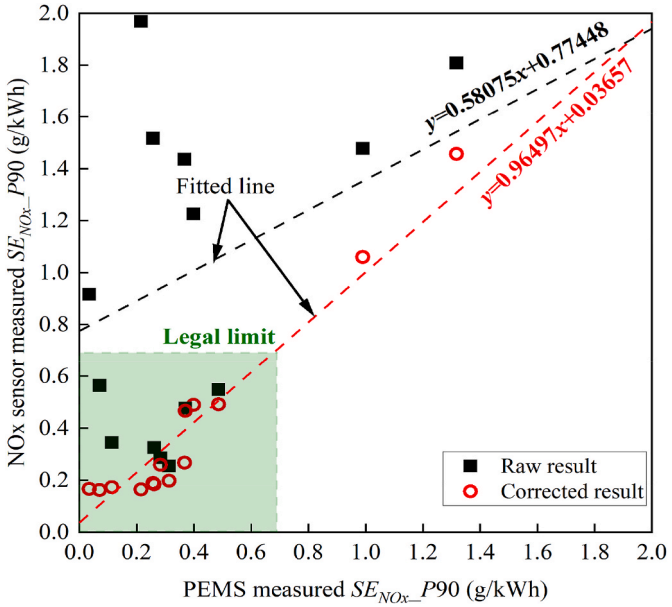

Fig. 16. Distribution of absolute SE_{NOx}_P90 errors before and after correction.

4. Discussion

To facilitate integration with existing regulatory telematics monitoring systems, the proposed framework can be implemented through the following workflow.

(1) Data Acquisition. Standardized OBD data streams are continuously acquired via existing telematics systems. Data are transmitted at fixed intervals to a central cloud platform.
(2) Cloud-Based Preprocessing. Upon data arrival, the system performs time synchronization and quality checks. Missing or invalid values are addressed through interpolation or flagged for exclusion. For each vehicle, a pre-trained LSTM model (or a lightweight surrogate model) estimates the UWS injection rate based on input features. To mitigate computational burden, LSTM inference can be performed in batch mode (e.g., weekly) rather than in real-time.
(3) Algorithm Execution. For each vehicle and each time window (e.g., the 10-s observation window used in this study), EI_{NH3} is calculated based on cumulative UWS and upstream NOx mass. The dual-condition slip identification logic (Fig. 10) is applied to detect NH_3 slip events. During confirmed slip periods, the downstream NOx sensor readings are corrected using a fixed 99% efficiency assumption (Eq. (10)).
(4) Periodic Model Updates. As new data become available, the LSTM model can be periodically retrained to adapt to fleet evolution and improve accuracy. Alternatively, a global model trained on a diverse dataset could be deployed across all vehicles, eliminating the need for vehicle-specific training.

The computational demands of the framework are modest and well-suited for large-scale deployment. The LSTM model inference is highly efficient: in our prototype implementation using Python with TensorFlow Lite on a standard server-grade CPU (AMD EPYC 7H12), processing 100,000 s of data (approximately 27.8 h of driving) takes 6.8 s. The sliding-window calculations for EI_{NH3} and slip detection add negligible overhead. For a fleet of one million vehicles, processing one day's data (assuming 4 h of operation per vehicle) would require approximately 272 CPU-core hours, which is well within the capacity of modern cloud computing platforms (e.g., 100 parallel cores could complete the task in ~2.7 h). The framework is therefore highly scalable and cost-effective for national or regional regulatory implementation.

While the framework has been validated on vehicles with similar aftertreatment architectures, its core principles, the mass-balance-derived EI_{NH3} and the dual-condition slip identification logic, are grounded in universal physical and chemical relationships, ensuring platform-agnostic applicability and satisfactory accuracy across diverse vehicle types. Nevertheless, for applications demanding even higher precision on specific vehicle platforms, the algorithm can be further tailored in two respects: first, the empirical thresholds (e.g., $EI_{NH3} > 0$ and efficiency $< 98\%$) can be recalibrated to account for variations in catalyst formulation or aging state. second, the LSTM model for UWS prediction can be retrained on vehicle-specific data or replaced with a more generalizable surrogate model to better capture unique dosing characteristics. Future work should broaden validation across additional vehicle classes, engine ages, and climatic conditions, and assess integration of the correction layer into standardized regulatory telematics data-processing pipelines to facilitate widespread adoption and maxi-

mize environmental benefits.

5. Conclusions

This study has developed and validated a novel telematics-integrated, dual-algorithm framework to mitigate NH_3-induced cross-sensitivity in NOx sensor measurements from heavy-duty diesel vehicles. The framework comprises an NH_3 slip identification module based on moving-window analysis of EI_{NH3} and SCR efficiency, and a correction module that applies a fixed 99% SCR conversion efficiency to confirmed slip events. The main conclusions are summarized as follows:

Under motorway high-speed operation, NH_3 slip deteriorates markedly due to the increased space velocity and elevated exhaust temperature. Across real-driving emission tests, the identification algorithm achieved high recall (77-97%) and accuracy (>93%), enabling reliable localization of periods in which NOx sensor signals are compromised and providing a prerequisite for selective correction. After correction, the characteristic positive bias caused by NH_3 slip was effectively reduced. For the key compliance metric SE_{NOx}_P90, the mean absolute error reduced by 94%, from 0.50 g/kWh to 0.03 g/kWh. Moreover, the distribution of errors narrowed substantially, indicating greatly improved measurement precision. In multi-vehicle evaluation, the framework can effectively correct false exceedances above the legal limit attributable to uncorrected sensor bias, reducing the risk of unjustified non-compliance determinations and improving the credibility of remote monitoring programs. The proposed approach is well suited for large-scale deployment because it requires no hardware modifications, relies only on data streams typically available via onboard telematics, and uses computationally lightweight algorithms compatible with retrospective, fleet-wide processing. Overall, the framework bridges the gap between laboratory certification and real-world emissions surveillance by providing a physically motivated, operationally feasible tool to restore NOx measurement fidelity, thereby supporting more reliable compliance verification and more accurate emissions assessment for data-driven air-quality management.

CRediT authorship contribution statement

Chuntao Liu: Writing – original draft, Investigation, Formal analysis. **Chenxi Wang:** Writing – review & editing, Visualization, Methodology, Formal analysis, Conceptualization. **Zhiqiang Li:** Writing – original draft, Investigation, Formal analysis. **Yiqiang Pei:** Supervision, Project administration. **Chunling Wu:** Investigation, Formal analysis. **Fan Zhang:** Methodology, Investigation. **Jing Qin:** Methodology, Investigation.

Declaration of competing interest

The authors declare that they have no known competing financial interests or personal relationships that could have appeared to influence the work reported in this paper.

Acknowledgement

This work was financially supported by the Key Technologies Research and Development Program (CN) (Grant No. 2022YFC3701805 and 2022YFC3703600) and technically supported by the CATARC Automotive Test Center Company Limited (Tianjin). The authors thank Guomin Pang and Weilin Liu of the CATARC Automotive Test Center Company Limited for their contribution to this program's emissions testing.

Data availability

The authors do not have permission to share data.

References

Aliramezani, M., Koch, C.R., Hayes, R.E., 2016. Estimating tailpipe NOx concentration using a dynamic NOx/ammonia cross sensitivity model coupled to a three state control oriented SCR model. IFAC-PapersOnLine 49 (11), 8–13. https://doi.org/10.1016/j.ifacol.2016.08.002.

Barbier, A., Salavert, J.M., Palau, C.E., et al., 2024. Analysis of the Euro 7 on-board emissions monitoring concept with real-driving data. Transp. Res., Part D Transp. Environ. 127, 104062. https://doi.org/10.1016/j.trd.2024.104062.

Birkhold, F., Meingast, U., Wassermann, P., et al., 2007. Modeling and simulation of the injection of urea-water-solution for automotive SCR DeNOx-systems. Appl. Catal. B Environ. 70 (1-4), 119–127. https://doi.org/10.1016/J.APCATB.2005.12.035.

California Air Resources Board (CARB), 2021. Clean truck check (HD I/M). Board Approved December 9, 2021.

Childress, B., Chen, P., 2018. A decomposition algorithm for a class of nonlinear dynamic systems with cross-sensitive output measurement. In: 2018 IEEE Conference on Decision and Control (CDC). IEEE. https://doi.org/10.1109/CDC.2018.8619717.

Engelmann, D., Zimmerli, Y., Ruoss, F., et al., 2021. Real driving emissions of diesel and LNG euro VI heavy-duty vehicles measured with FTIR-PEMS. SAE Tech. Pap. 2021-24-0066. https://doi.org/10.4271/2021-24-0066.

Feng, T., Lu, L., 2015. The characteristics of ammonia storage and the development of model-based control for diesel engine urea-SCR system. J. Ind. Eng. Chem. 28, 97–109. https://doi.org/10.1016/j.jiec.2015.02.004.

Feng, Q., Zhen, K., Lu, Y., et al., 2021. Analysis on emission characteristics of urban buses based on remote online monitoring. SAE Tech. Pap. 2021-01-0601. https://doi.org/10.4271/2021-01-0601.

Funk, S., 2021. Real world NOx sensor accuracy assessment and implications for real NOx tracking. SAE Int. J. Adv. & Curr. Pract. Mobil. 3 (6), 2761–2769. https://doi.org/10.4271/2021-01-0593.

Ge, Y., Hou, P., Lyu, T., et al., 2023. Machine learning-aided remote monitoring of NOx emissions from heavy-duty diesel vehicles based on OBD data streams. Atmosphere 14 (4), 651. https://doi.org/10.3390/atmos14040651.

Ge, Z., Li, W., Wang, J., et al., 2025. Real-road NOx and CO_2 emissions of city and highway China-6 heavy-duty diesel vehicles. J. Environ. Sci. 149, 330–341. https://doi.org/10.1016/j.jes.2023.11.018.

He, L., Li, G., Wu, X., et al., 2024. Characteristics of NOX and NH3 emissions from in-use heavy-duty diesel vehicles with various aftertreatment technologies in China. J. Hazard Mater. 465, 133073. https://doi.org/10.1016/j.jhazmat.2023.133073.

Helyar, S., Alnaggar, A., 2025. Air quality monitoring and mitigation through time series forecasting and stochastic optimization. J. Environ. Manag. 389, 125540. https://doi.org/10.1016/j.jenvman.2025.125540.

Hu, J., Zhao, Y., Zhang, Y., et al., 2011. Development of closed-loop control strategy for urea-SCR based on NOx sensors. SAE Tech. Pap. 2011-01-1324. https://doi.org/10.4271/2011-01-1324.

Huang, Y., Mok, W.C., Yam, Y.S., et al., 2020. Evaluating in-use vehicle emissions using air quality monitoring stations and on-road remote sensing systems. Sci. Total Environ. 740, 139868. https://doi.org/10.1016/j.scitotenv.2020.139868.

Jeong, J.W., Cha, J., Chon, M.S., et al., 2023. Suitability of SEMS equipment for monitoring RDE tests. Int. J. Automot. Technol. 24 (3), 749–758. https://doi.org/10.1007/s12239-023-0062-1.

Jiang, Y., Tan, Y., Yang, J., et al., 2022. Understanding elevated real-world NOx emissions: Heavy-duty diesel engine certification testing versus in-use vehicle testing. Fuel 307, 121771. https://doi.org/10.1016/j.fuel.2021.121771.

Jones, J.C.P., Geveci, M., 2011. Smart sensing and decomposition of NOx and NH3 components from production NOx sensor signals. SAE Tech. Pap. 2011-01-1157. https://doi.org/10.4271/2011-01-1157.

Komnos, D., Smit, R., Ntziachristos, L., Fontaras, G., 2025. A comparative analysis of car fleet efficiency evolution in Europe and Australia insights on policy influence. J. Environ. Manag. 373, 123313. https://doi.org/10.1016/j.jenvman.2024.123313.

Liu, C., Pei, Y., Wu, C., et al., 2023. Novel insights into the NOx emissions characteristics in PEMS tests of a heavy-duty vehicle under different payloads. J. Environ. Manag. 348, 119400. https://doi.org/10.1016/j.jenvman.2023.119400.

Opitz, B., Bendrich, M., Drochner, A., et al., 2015. Simulation study of SCR catalysts with individually adjusted ammonia dosing strategies. Chem. Eng. J. 264, 936–944. https://doi.org/10.1016/j.cej.2014.11.114.

Smit, R., Kingston, P., Neale, D.W., et al., 2019. Monitoring on-road air quality and measuring vehicle emissions with remote sensing in an urban area. Atmos. Environ. 218, 116978. https://doi.org/10.1016/j.atmosenv.2019.116978.

Todo, Y., Ichikawa, H., Yotou, H., Aoki, K., et al., 2018. Development of high accuracy and quick light-off NOx sensor. SAE Tech. Pap. 2018-01-0334. https://doi.org/10.4271/2018-01-0334.

Van Nieuwstadt, M., 2022. On the utility of ammonia sensors for diesel emissions control. SAE Tech. Pap. 2022-01-0549. https://doi.org/10.4271/2022-01-0549.

Wang, H., Wu, Y., Zhang, K., et al., 2020a. Evaluating mobile monitoring of on-road emission factors by comparing concurrent PEMS measurements. Sci. Total Environ. 736, 139507. https://doi.org/10.1016/j.scitotenv.2020.139507.

Wang, C., He, K., Fang, X., et al., 2020b. Design and implementation of emission monitoring platform for heavy duty diesel vehicles. In: 2020 International Conference on Computer Science and Management Technology (ICCSMT). IEEE, pp. 336–339. https://doi.org/10.1109/ICCSMT51754.2020.00076.

Wang, Y., Yin, H., Wang, J., et al., 2022. China 6 moving average window method for real driving emission evaluation: challenges, causes, and impacts. J. Environ. Manag. 319, 115737. https://doi.org/10.1016/j.jenvman.2022.115737.

Xia, Y., Jiang, L., Wang, L., et al., 2022. Rapid assessments of light-duty gasoline vehicle emissions using on-road remote sensing and machine learning. Sci. Total Environ. 815, 152771. https://doi.org/10.1016/j.scitotenv.2021.152771.

Xu, J., Lu, M., Guo, Y., et al., 2023. Summertime urban ammonia emissions may be substantially underestimated in Beijing, China. Environ. Sci. Technol. 57 (35), 13124–13135. https://doi.org/10.1021/acs.est.3c05266.

Yan, F., Wei, L., Hu, J., et al., 2019. Simultaneous optimization of urea dosing and ammonia coverage ratio of selective catalytic reduction system in diesel engine by using physico-chemical model based NSGA-II algorithm. Appl. Therm. Eng. 154, 46–62. https://doi.org/10.1016/j.applthermaleng.2019.03.031.

Yang, S., Feng, S., Sun, K., et al., 2020. Square-root unscented Kalman filter for ammonia coverage ratio and input ammonia estimations in diesel-engine urea-SCR system. ISA Trans. 96, 299–308. https://doi.org/10.1016/j.isatra.2019.06.025.

Yang, Z., Rushton, C., Tate, J., 2025. Detected or not? Remote sensing measurements from the latest Euro 6d vehicles across Europe. J. Environ. Manag. 395, 127767. https://doi.org/10.1016/j.jenvman.2025.127767.

Yu, Y.S., Jeong, J.W., Chon, M.S., et al., 2021. NOx emission of a correlation between the PEMS and SEMS over different test modes and real driving emission. Energies 14 (21), 7250. https://doi.org/10.3390/en14217250.

Zhang, S., Zhao, P., He, L., et al., 2020. On-board monitoring (OBM) for heavy-duty vehicle emissions in China: regulations, early-stage evaluation and policy recommendations. Sci. Total Environ. 731, 139045. https://doi.org/10.1016/j.scitotenv.2020.139045.

Zhang, W., Fang, X., Sun, C., 2023. The alternative path for fossil oil: electric vehicles or hydrogen fuel cell vehicles? J. Environ. Manage. 341, 118019. https://doi.org/10.1016/j.jenvman.2023.118019.

Zhao, Y., Hu, J., Hua, L., et al., 2011. Ammonia storage and slip in a urea selective catalytic reduction catalyst under steady and transient conditions. Ind. Eng. Chem. Res. 50 (21), 11863–11871. https://doi.org/10.1021/ie201045w.

Zhao, P., Wu, X., Zhang, S., et al., 2024. Regulatory insights for on-board monitoring of vehicular NOx emission compliance. Environ. Sci. Technol. 58 (18), 7968–7976. https://doi.org/10.1021/acs.est.4c00079.